

**Translating Electrocardiograms to Cardiac Magnetic Resonance Imaging Useful for
Cardiac Assessment and Disease Screening: A Multi-Center Study
AI for ECG to CMR Translation Study**

Zhengyao Ding^{1*}, Ziyu Li^{1*}, Yujian Hu^{2*}, Youyao Xu⁵, Chengchen Zhao⁶, Yiheng Mao¹, Haitao Li¹,
Zhikang Li¹, Qian Li,⁴ Jing Wang³, Yue Chen³, Mengjia Chen³, Longbo Wang³, Xuesen Chu⁷, Weichao
Pan⁸, Ziyi Liu⁸, Fei Wu^{1,#}, Hongkun Zhang^{2,#}, Ting Chen^{3,#}, Zhengxing Huang^{1,#}

¹ College of Computer Science and Technology, Zhejiang University, Hangzhou, China

² Department of Vascular Surgery, The First Affiliated Hospital of Zhejiang University School of Medicine, Hangzhou, China

³ Department of Cardiology, The First Affiliated Hospital, Zhejiang University School of Medicine, Hangzhou, Zhejiang Province, China

⁴ Department of Radiology, The First Affiliated Hospital, Zhejiang University School of Medicine, Hangzhou, Zhejiang Province, China

⁵ Department of Vascular Surgery, Quzhou People's Hospital, Quzhou, China

⁶ Department of Cardiology, The Second Affiliated Hospital of Zhejiang University School of Medicine, Hangzhou, China

⁷ China Ship Scientific Research Center, Wuxi, China

⁸ Guangdong Transtek Medical Electronics Co., Ltd., Zhongshan, China

Corresponding authors

* These authors contributed equally to this work.

Abstract

Background:

Cardiovascular diseases (CVDs), the leading cause of global mortality, require early and accurate diagnosis to improve outcomes. Cardiac magnetic resonance imaging (CMR) provides gold-standard functional and structural insights but remains inaccessible due to cost and complexity. Electrocardiography (ECG) is widely available but lacks CMR's granularity. We propose **CardioNets**, a deep learning framework that translates 12-lead ECG data into functional parameters and synthetic images closely aligned with CMR imaging, enabling scalable, low-cost cardiac assessment.

Methods:

CardioNets combines cross-modal contrastive learning and generative pretraining to link ECG signals with CMR-derived cardiac phenotypes (e.g., ejection fraction, myocardial mass). The framework operates in two phases: (1) Cross-modal alignment, where ECG is aligned with CMR functional data, and (2) CMR image synthesis, where a masked autoregressive model generates high-fidelity CMR images from ECG input. The model was trained and validated on 159,819 samples from five cohorts, including the UK Biobank (n=42,483) and MIMIC-IV-ECG (n=164,550), with external testing on two independent clinical datasets (n=3,767). Tasks included multi-disease screening (e.g., cardiomyopathy, coronary artery disease) and cardiac function assessment.

Findings:

In the UK Biobank, CardioNets improved cardiac phenotypes regression R^2 by 24.8% over model trained from scratch and 12.3% over self-supervised pretraining, and boosted cardiomyopathy screening AUC by 39.3% and 6.3%, respectively. In MIMIC, it raised AUC for pulmonary hypertension screening by 5.6% over model trained from scratch. Synthesized CMR images by CardioNets showed 36.6% higher SSIM and 8.7% higher PSNR than prior method. In the reader study, cardiomyopathy screening using CardioNets (ECG only) achieved a 13.9% higher accuracy compared to the average performance of human physicians using both ECG and real CMR. In most disease-screening tasks, CardioNets performance closely matched CMR-based models, demonstrating ECG's potential as a low-cost surrogate for CMR in cardiovascular screening.

Interpretation:

CardioNets bridges the accessibility gap between ECG and CMR, offering a cost-effective solution for population-scale screening. By translating ECG into CMR-level insights, CardioNets bridges gaps in accessibility and interpretability, enabling population-scale screening without compromising diagnostic accuracy. The model's ability to generate CMR images from ECG enhances clinical decision-making, particularly in resource-limited settings. Future work should validate real-world implementation and regulatory pathways for AI-generated imaging.

Research in Context

Evidence before this study

Cardiovascular diseases (CVDs) are the leading cause of global mortality, yet early diagnosis remains a challenge due to the limitations of current diagnostic tools. Electrocardiography (ECG) is cost-effective, widely accessible, and commonly used in clinical settings. However, it primarily detects electrical abnormalities and is unable to evaluate structural or functional heart issues. In contrast, cardiac magnetic resonance imaging (CMR) offers a comprehensive assessment of heart structure and function, but its high cost, complexity, and limited availability make it inaccessible, particularly in resource-limited settings. Although few prior studies have attempted to integrate ECG and CMR, they struggled to effectively identify structural heart diseases and lacked the capacity to generate high-fidelity CMR images. The potential for integrating ECG with CMR through cross-modal artificial intelligence (AI) remains an underexplored area of research.

Added value of this study

This study introduces CardioNets, a new cross-modal AI framework that translates standard 12-lead ECG data into diagnostic CMR-derived functional parameters and synthetic CMR images. By leveraging contrastive learning, CardioNets aligns ECG waveforms with CMR biomarkers, such as ejection fraction and global longitudinal strain. Additionally, it employs a masked autoregressive model to generate high-quality CMR images from ECG data. Trained on extensive datasets like the UK Biobank and MIMIC-IV, CardioNets significantly enhances ECG's ability to detect structural heart diseases, with performance comparable to CMR-based diagnostic models. External reader study showed a 13.9% accuracy gain with CardioNets over physicians using ECG and real CMR.

Implications of all available evidence

CardioNets bridges the accessibility gap between ECG and CMR, offering a cost-effective solution for early CVD detection in resource-limited regions. The synthetic CMR images generated by CardioNets enhance interpretability, facilitating informed decision-making without the need for specialized imaging. From a policy perspective, this AI-driven model offers a cost-effective and scalable solution for population-level screening of non-communicable diseases, aligning with global health objectives. In the long term, CardioNets could reduce unnecessary CMR referrals, expedite diagnostic processes, and provide a framework for the application of AI in other resource-constrained diagnostic domains.

Introduction

Cardiovascular diseases (CVDs) remain the leading cause of mortality worldwide, with their share of global deaths increasing significantly in recent years¹⁻³. Among these, the mortality rate associated with cardiomyopathy has risen by 7.6%, significantly contributing to the growing burden of cardiovascular disease⁴. The clinical presentation of CVDs is often complex and multifactorial, leading to missed or misdiagnosed cases, which can delay treatment and compromise patient care^{5,6}. To effectively assess cardiovascular health, clinicians utilize a variety of diagnostic modalities, including electrocardiography (ECG)⁷ and cardiovascular magnetic resonance imaging (CMR)⁸. ECG measures the electrical activity of the heart, helping identify conditions like myocardial infarction and arrhythmias. It is widely adopted due to its non-invasive nature, low cost, and accessibility across healthcare settings. However, while ECG offers valuable insights into electrical abnormalities, it has limitations in assessing structural and functional cardiac conditions⁹. On the other hand, CMR provides a more comprehensive evaluation, offering detailed imaging of cardiac morphology, function, myocardial perfusion, and tissue characterization¹⁰⁻¹³, making it especially valuable in assessing structural heart diseases like cardiomyopathy¹⁴⁻¹⁶. Despite its strengths, CMR’s high costs and operational complexity limit its accessibility, particularly in resource-constrained settings¹⁷. This discrepancy highlights the urgent need for methods that can enhance ECG’s diagnostic power, particularly as a preliminary tool for CVD screening.

Recent advancements in large-scale multimodal datasets, such as the UK Biobank (UKB) and MIMIC^{18,19}, coupled with breakthroughs in deep learning, offer a transformative opportunity to address this gap. Cross-modal contrastive learning approaches, exemplified by CLIP (Contrastive Language-Image Pre-training)²⁰, have demonstrated the ability to align diverse data modalities and enable high-precision tasks like zero-shot classification, where models can make predictions without task-specific training. Additionally, generative models, such as autoregressive model^{21,22} and stable diffusion model²³, have harnessed CLIP’s text encoder to guide the generation of high-fidelity images from textual descriptions, further expanding the potential of cross-modal models in healthcare. These advances pave the way for integrating ECG and CMR in innovative ways that could improve disease detection and treatment planning²⁴⁻²⁶.

In response to these challenges and opportunities, we introduce **CardioNets**, a novel approach that utilizes cross-modal alignment and generative pretraining to enhance cardiac assessment. Unlike traditional methods, which align text-image pairs of similar content²⁰, CardioNets focuses on strengthening the relationship between a more robust modality (CMR) and a weaker modality (ECG) to improve the latter’s performance. While prior studies have explored joint analysis of ECG and CMR data²⁴, CardioNets is uniquely designed to improve screening for structural heart diseases, such as cardiomyopathy, by aligning ECG signals with corresponding CMR images through contrastive learning. This process enriches the ECG data, allowing for more accurate cardiac evaluations. Additionally, CardioNets incorporates a generative model²⁷ to generate dynamic CMR sequences from ECG data, improving interpretability and aiding clinical decision-making.

We evaluate CardioNets across two phases: (1) cross-modal learning and ECG-based CMR image generation, and (2) downstream cardiac assessments, including cardiac phenotype prediction and screening for coronary artery disease, heart failure, cardiomyopathy, and pulmonary arterial hypertension. In the UK Biobank, CardioNets improved cardiac phenotypes regression R^2 by 24.8%

over model trained from scratch and 12.3% over model trained from self-supervised pretraining, and boosted cardiomyopathy screening AUC by 39.3% and 6.3%, respectively. In MIMIC, it raised AUC for pulmonary hypertension screening by 5.6% over model trained from scratch. Synthesized CMR images by CardioNets showed 36.6% higher SSIM and 8.7% higher PSNR than prior method²⁴. A reader study also demonstrated the practical utility of CardioNets, particularly in aiding resident and attending physicians in cardiomyopathy screening. In conclusion, CardioNets offers a scalable, cost-effective solution for early CVD detection, with the potential to transform clinical practice, particularly in settings with limited access to advanced imaging technologies.

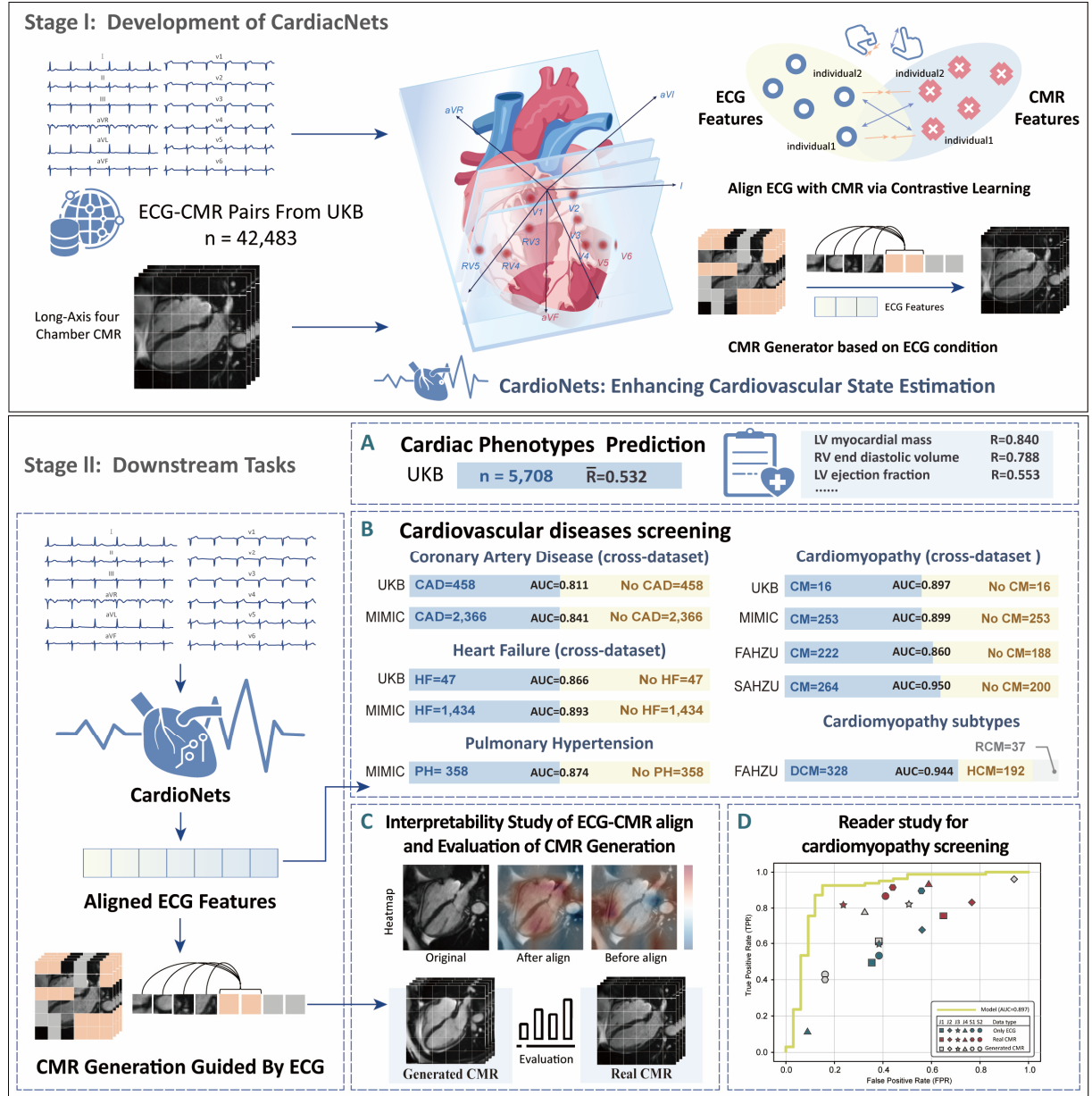


Fig. 1: Overview of the study design. **Stage I:** Development of CardioNets. Using the UKB dataset, we trained two core components of CardioNets: (1) an ECG model trained with ECG-CMR contrastive learning to capture relevant information from CMR, and (2) a CMR generation model trained with a masked autoregressive model conditioned on ECG. **Stage II:** Downstream tasks. The datasets used are from UKB, MIMIC-IV-ECG, The First Affiliated Hospital of Zhejiang University School of Medicine (FAHZU), The Second Affiliated Hospital of Zhejiang University School of Medicine (SAHZU). All numbers annotated in

the figure are test set sample sizes. All tasks used only ECG data to validate the model's performance, including: (A) Prediction of cardiac phenotypes, (B) Screening for cardiovascular diseases, particularly cardiomyopathy, (C) Interpretability study of ECG-CMR align and evaluation of CMR generation, and (D) Reader study for cardiomyopathy screening.

Methods

Dataset for Model Development and Evaluation

We used the UK Biobank (UKB) ¹⁸, the largest publicly available dataset of paired ECG and cine CMR imaging, for model development. The UKB contains data from 500,000 participants aged 40–69, recruited across the UK since 2006, with ongoing data collection. Our focus was on ECG-CMR pairs from participants’ initial imaging visits, totalling 42,483 paired samples. The ECG data includes 12-lead recordings, 10 seconds long, sampled at 500 Hz. The cine CMR data consists of four-chamber long-axis views, each with 50 frames capturing a single cardiac cycle. The dataset is 48.3% male and 51.7% female, with the majority (96.6%) identifying as White. Smaller ethnic groups include Mixed (0.5%), Asian (1.1%), Black (0.7%), Chinese (0.3%), and others (0.5%). Ethnicity data follows the UKB Data-Coding system (1001), with 0.3% of participants not disclosing their ethnicity. The dataset was split into training, validation, and test sets in a 70:10:20 ratio, supporting the development and evaluation of our Contrastive ECG-CMR Pre-training and ECG2CMR generative Models.

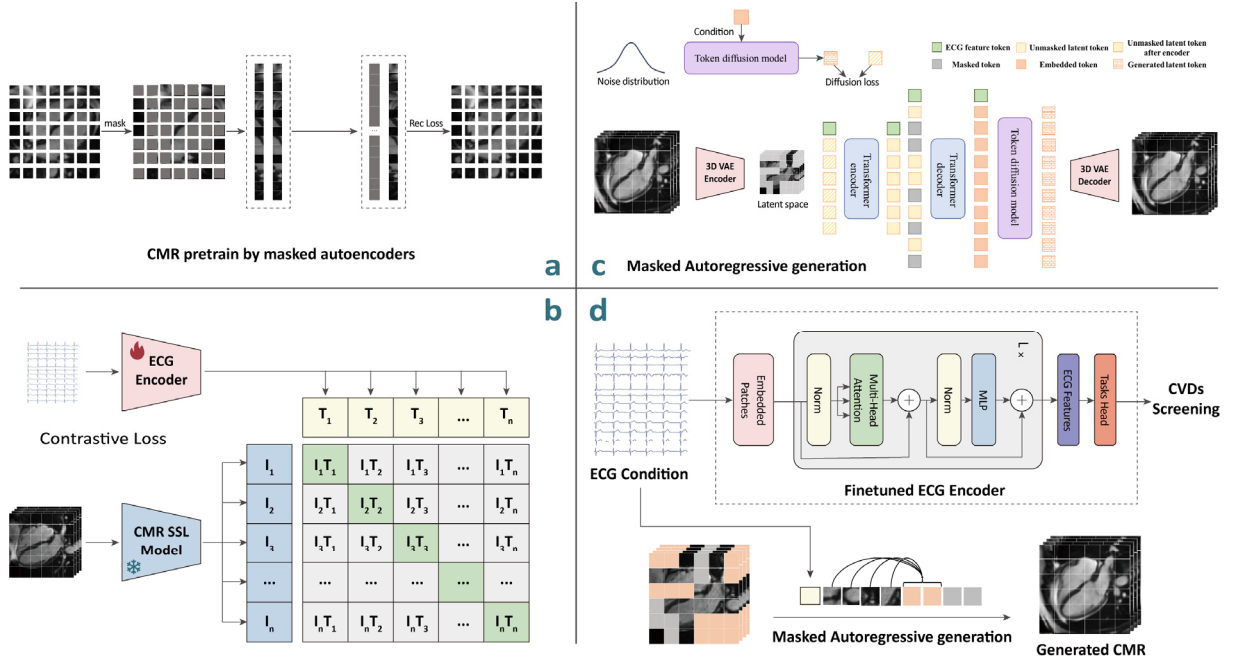


Fig. 2: Model diagram. **a.** CMR self-supervised model, leveraging the masked self-supervised learning, optimized to minimize reconstruction loss. **b.** ECG-CMR contrastive learning, with the parameters of the CMR self-supervised model in **subgraph a** frozen, optimized to minimize contrastive loss. **c.** ECG-guided CMR image generation, using the pre-trained ECG encoder in **subgraph b** as the feature extractor. **d.** Finetuning the aligned ECG encoder to adapt to various downstream tasks and use pretrained generative model in **subgraph c** generate the corresponding CMR images.

For our downstream analyses, we used the UKB, MIMIC-IV-ECG²⁸, and private datasets from two hospitals: the First and Second Affiliated Hospitals of Zhejiang University School of Medicine (FAHZU, SAHZU):

In the UKB dataset, 2,604 CVD individuals and 26,040 non-CVD controls were chosen. From MIMIC-IV-ECG, we selected 22,047 CVD samples and 118,300 non-CVD controls. In UKB dataset, we adopted five-fold cross-validation to assess model performance. We reported the average performance and its variability as the mean \pm standard deviation across the five folds. For statistical significance testing—

including p-values, confidence intervals, and effect sizes—we aggregated all validation samples from the five folds into a unified evaluation set (Extended Fig. 2). This pooled approach facilitates consistent and robust model comparisons, though the resulting AUC may differ slightly from the cross-validation mean due to changes in sample distribution and weighting. For the larger MIMIC dataset, we adopted a 60:20:20 split for training, validation, and testing, reporting results on the held-out test set with 95% confidence intervals (CIs) computed using the Wilson score interval. Both MIMIC and UKB ECG data are recorded at 500 Hz for 10 seconds. Our focus was on classifying several cardiovascular conditions, including coronary artery disease (CAD), pulmonary hypertension, cardiomyopathy, and heart failure, as defined by ICD-10 codes. In addition to constructing a balanced dataset with a 1:1 ratio of non-CVD controls to CVD cases²⁹, we further evaluated the model under more clinically realistic settings with imbalance ratios of 2:1, 5:1, and 10:1 to assess its robustness. Additionally, we aimed to predict 82 cardiac structural phenotypes (Supplementary Table 8). Pulmonary hypertension cases were excluded from UKB due to their low frequency. MIMIC-IV-ECG lacks corresponding CMR images, so cardiac structural indicator assessment was not possible.

For private datasets, the FAHZU dataset is divided into three subsets: Subset 1: ECG data for a three-class cardiomyopathy classification, including 1,705 cases of dilated cardiomyopathy (DCM), 915 cases of hypertrophic cardiomyopathy (HCM), and 162 cases of restrictive cardiomyopathy (RCM). We reported five-fold cross-validation results as mean \pm standard deviation, and conducted statistical significance testing (p-value, confidence interval, and effect size) on the pooled validation set, consistent with the procedure used in the UKB dataset. Subset 2: ECG data for external validation of cardiomyopathy, with 222 cardiomyopathy patients and 188 controls. Subset 3: ECG-CMR paired data for a reader study, consisting of 77 cardiomyopathy patients and 34 controls. The SAHZU dataset includes 264 cardiomyopathy patients and 200 controls. The FAHZU subset 2 and the SAHZU dataset were used for external validation of cardiomyopathy, with 95% confidence intervals (CIs) of the evaluation metric (AUC) computed using the Wilson score interval. All datasets utilize the same ECG format as the UKB dataset. Data distributions are provided in Supplementary Table 9-11.

Data processing and augmentation

We applied a series of signal pre-processing techniques to enhance the quality and reliability of the ECG data. Baseline drift was corrected using seasonal decomposition, isolating and removing the trend component. Noise reduction was achieved with wavelet transform denoising using the “db6” wavelet and soft thresholding, preserving key signal characteristics. Finally, the Savitzky-Golay filter³⁰ smoothed the signal using polynomial fitting within a sliding window. These steps ensured clean and reliable data for robust analysis.

For long-axis four-chamber CMR images, we applied a pretrained segmentation model³¹ to generate heart region masks. Images were then cropped to 96×96 pixels based on the minimal bounding box of the masks to capture the relevant cardiac structures. Each image sequence was represented as a three-dimensional structure with 50-time frames.

In the Contrastive ECG-CMR pre-training and downstream tasks, data augmentation techniques were applied. ECG data was augmented with crop resizing, time reversal (TimeFlip), and sign inversion (SignFlip), followed by Min-Max scaling. For CMR images, random rotation (up to 30 degrees), random flips, and random resized cropping (scale range of 0.8 to 1.0 and aspect ratio of 0.9 to 1.1) were applied.

During validation and testing, only Min-Max scaling for ECG data and normalization and resizing for CMR images were used. During the training phase of the ECG2CMR generative model, we preserved critical data features by applying only Min-Max scaling to ECG data and resizing to CMR images.

Self-supervised method for CMR

We applied self-supervised learning to CMR images to obtain robust representations, enabling contrastive ECG-CMR pretraining (Fig. 2a). A large volume of phenotype-conditioned synthetic CMR images generated via CPGG³² was mixed with real CMR data (mix 500%) for masked self-supervised training³³. We employed a Vision Transformer (ViT) as the backbone, using a patch size of 16×16 . The temporal dimension of the long-axis cine CMR (50 frames) was treated as the channel dimension, with random masking applied across channels at a ratio of 75%. The model was trained to reconstruct the masked inputs using a reconstruction loss. Training was conducted on an 80 GB A800 GPU with a batch size of 32 for 400 epochs. The first 40 epochs were dedicated to learning rate warm-up, linearly increasing from 0 to 1×10^{-4} . Final model checkpoints were saved for downstream tasks.

Contrastive ECG-CMR Pre-training

Building on the pretrained CMR encoder (with its parameters frozen), we initialized the ECG encoder using weights from the ST-Mem self-supervised model³⁴. We then aligned the features of ECG and CMR images in the latent space using a contrastive learning approach (Fig. 2b). During the forward pass, the model computes the logits as follows:

$$\text{logits} = \frac{\text{hidden1} \cdot \text{hidden2}^T}{\text{temperature}} \quad (1)$$

Here, *hidden* and *hidden2* represent the feature embeddings of the ECG and CMR images, respectively, and the temperature parameter is set to 0.05. The contrastive loss was then calculated in both directions, consisting of the following Equations (2-3):

$$\text{zis_findmostgood_zjs} = \text{F.cross_entropy}(\text{logits}, \text{label}) \quad (2)$$

$$\text{zjs_findmostgood_zis} = \text{F.cross_entropy}(\text{logits}^T, \text{label}) \quad (3)$$

Here, *label* is a diagonal matrix, where each diagonal element corresponds to a positive pair (ECG-CMR pair), while the off-diagonal elements are set to 0, indicating negative pairs. The final loss is then computed as:

$$\text{loss} = 0.5 \cdot \text{zis_findmostgood_zjs} + 0.5 \cdot \text{zjs_findmostgood_zis} \quad (4)$$

The model was trained on an 80GB A800 GPU with a batch size of 256 for up to 400 epochs. The first 40 epochs focused on learning rate warm-up, gradually increasing the learning rate from 0 to 1×10^{-3} . The model checkpoint with the lowest validation loss was saved for use in downstream tasks.

ECG2CMR masked autoregressive generative model

Similar to Stable Diffusion²³, our model performs generation in the latent space. We employ a 3D Variational Autoencoder (3D-VAE) as the compressor for CMR data, with spatial and temporal downsampling rates denoted as f_s and f_t , respectively. For a long-axis cine CMR input of shape

$(1, T, H, W)$, the resulting latent representation x has dimensions of $|x| \times \frac{T}{f_t} \times \frac{H}{f_s} \times \frac{W}{f_s}$, where $|x|$ denotes the latent dimensionality.

For the ECG-to-CMR generative model, we build upon the Masked Autoregressive Model (MAR)²². The MAR is a variant of the standard autoregressive model that enables simultaneous prediction of multiple tokens conditioned on the observed ones, offering improved efficiency and flexibility over conventional step-by-step autoregressive approaches. This autoregressive process can be formulated as:

$$P(X_1, \dots, X_K) = \prod_{k=1}^K P(X_k | X_1, \dots, X_{k-1}), X_k = \{x_1, \dots, x_i\} \quad (5)$$

where X_k represents the set of tokens predicted at the k -th step, x_i denotes an individual token. We employ a Transformer network with bidirectional attention as the backbone of the autoregressive model. Specifically, the compressed CMR representations produced by the 3D-VAE encoder are partitioned into non-overlapping tokens of shape $|x| \times p_t \times p_s \times p_s$, where $p_t \times p_s$ are temporal and spatial strides, respectively. A dynamic masking ratio, as proposed²², is applied during training to randomly mask tokens.

To model the continuous distribution of individual tokens, we adopt a token-wise diffusion mechanism in latent space. Let x_i denote the ground-truth token and z_i represent the context-aware embedding generated by the autoregressive model up to position i , i.e., $z_i = f(X_1, \dots, X_{i-1})$. Our goal is to learn the conditional distribution $p(x_i | z_i)$, which we achieve by introducing a diffusion-based loss function:

$$\mathcal{L}(z_i, x_i) = \mathbb{E}_{\epsilon, t} \left[\|\epsilon - \epsilon_\theta(x_i^t | t, z_i)\|^2 \right] \quad (6)$$

, where $\epsilon \sim \mathcal{N}(0, I)$ is the noise vector, and x_i^t is the noisy version of the token at time step t , defined by the forward diffusion process: $x_i^t = \sqrt{\bar{\alpha}_t} x_i + \sqrt{1 - \bar{\alpha}_t} \epsilon$, with $\bar{\alpha}_t$ being part of a predefined noise schedule. The denoising function ϵ_θ is modeled using a lightweight MLP and is trained only on masked tokens. During inference, reverse sampling is applied from x_i^t back to x_i^0 using the following recursive formulation:

$$x_i^{t-1} = \frac{1}{\sqrt{\alpha_t}} \left(x_i^t - \frac{1 - \alpha_t}{\sqrt{1 - \bar{\alpha}_t}} \epsilon_\theta(x_i^t | t, z_i) \right) + \sigma_t \delta \quad (7)$$

, where $\delta \sim \mathcal{N}(0, I)$, and σ_t denotes the standard deviation of the noise at time step t .

We first encode the input ECG using the aligned ECG encoder to obtain ECG feature representations. These features are then prepended to the CMR token sequence as a special classification token (CLS token). A bidirectional attention mechanism is applied to this combined sequence, enabling each CMR token to integrate conditional information from the ECG and thereby facilitating ECG-guided CMR generation. For generation, we adopt an iterative decoding strategy³⁵ to synthesize the cine CMR sequence. The process begins with an empty latent representation of the CMR, where all tokens are initially masked. Iterative decoding is performed over K steps, where in each step the model predicts a subset of the remaining masked tokens. A portion of the predicted tokens is randomly retained, while the masking ratio follows a cosine schedule across iterations. This progressive refinement ensures that

the model gradually improves the quality of the generated CMR representations.

In our implementation, the 3D-VAE is configured with a latent dimensionality of 16, f_t of 2, and f_s of 8. For the masked autoregressive model, we employed a 12-layer encoder–decoder architecture with a latent embedding size of 768 and a patch size of $5 \times 2 \times 2$. The patch size was selected to reduce computational load, leveraging the inherent temporal redundancy of cine CMR data. During training, the masking ratio was randomly sampled between 0.7 and 1.0. For the diffusion component, we adopted a cosine-based noise schedule with 1,000 timesteps during training and 100 timesteps during inference. The noise prediction network consisted of a 3-block multilayer perceptron (MLP) with a channel width of 1,024. The iterative decoding process was performed over 16 steps to progressively reconstruct the CMR sequence. Experiments were conducted on an NVIDIA A800 GPU (80 GB). The models were trained using the AdamW optimizer with a learning rate of 8×10^{-4} for 400 epochs.

Downstream tasks

For downstream tasks, we used only the ECG encoder from the Contrastive ECG-CMR Pre-training model, excluding the CMR encoder (Fig. 2d). The ECG encoder extracts high-level features from ECG signals, embedding CMR information. The pre-trained autoregressive generative model (Fig. 2c) was used for generating high-fidelity CMR images with authentic cardiac details, providing valuable insights for clinicians. We fine-tuned the ECG encoder to match the data distributions of each task, except for external validation datasets where the trained model was used for inference. The objective was to generate classification outputs aligned with CVD labels or regression outputs close to the ground truth for 82 cardiac phenotypes. Training was conducted with a batch size of 16 for up to 100 epochs, using a learning rate of 5×10^{-5} with cosine annealing scheduling, a 10-epoch warm-up, and early stopping.

Quantitative assessment and statistical analysis

For classification tasks, we employed several evaluation metrics: area under the curve (AUC), accuracy, sensitivity, specificity, positive predictive value (PPV), and negative predictive value (NPV). In our three-class classification, we binarized the labels using a one-vs-rest approach prior to evaluation. For regression tasks related to cardiac phenotypes, we used the coefficient of determination (R^2), Pearson correlation coefficient, mean absolute error (MAE), and root mean squared error (RMSE) as the primary evaluation metrics. For the MIMIC dataset and the FAHZU and SAHZU external inference datasets, 95% confidence intervals (CIs) were computed using the Wilson Score Interval³⁶. For the UKB and FAHZU multiclass classification datasets, we reported the mean and std based on five-fold cross-validation. To compare CardioNets with baseline methods (model based CMR, Pretrained ECG model, and Scratch ECG model), we evaluated AUC, balanced accuracy, and mean average precision (mAP); statistical significance was assessed using the DeLong test for AUC, and permutation tests ($N = 10,000$) for balanced accuracy and mAP. In addition, 95% confidence intervals were estimated using bootstrap resampling with 10,000 iterations.

Software for data process and model development

We utilized several libraries for data processing and model development, including numpy (version 1.25.2)³⁷, sklearn (version 1.1.1)³⁸, scipy (version 1.11.2)³⁹, simpleITK (version 2.3.1)⁴⁰ and pandas (version 2.2.1). For model development, we employed pytorch (version 1.11.0).

Results

Cardiac assessments

We evaluated the performance of the fine-tuned CardioNets model using two public datasets (UKB, MIMIC) and two private datasets (FAHZU, SAHZU) for predicting cardiac structural phenotypes and cardiovascular disease (CVD) conditions (Fig. 3). In the UKB dataset, which contains paired CMR images, we compared CardioNets with both standalone ECG-based and CMR-based models. In contrast, due to the absence of corresponding CMR images in the MIMIC and private hospital datasets, comparisons were limited to ECG-based models and CardioNets. To ensure fairness in comparison, the ECG-based models comprised one trained from scratch and another fine-tuned from a self-supervised pretraining framework³⁴. The CMR-based model was likewise initialized with self-supervised pretraining³³ to maximize its representational capacity.

For cardiac phenotype prediction across 82 indicators (e.g., atrial ejection fractions and chamber volumes), CardioNets achieved an average coefficient of determination (R^2) of 0.302, outperforming both ECG-only baselines (0.269 and 0.242), though still below the performance of the CMR-based model (0.511). We further compared CardioNets with two recent state-of-the-art methods, Cross-AE²⁴ and MMCL⁴¹, and observed that CardioNets significantly outperformed both in predicting cardiac phenotypes (Supplementary Fig. 1).

For CVD screening, CardioNets demonstrated substantial improvements over both ECG-based baselines across three conditions—coronary artery disease (CAD), heart failure, and cardiomyopathy—in the UKB dataset. Notably, for cardiomyopathy detection, CardioNets outperformed the scratch-trained and pretrained ECG models by 39.3% and 6.3%, respectively. In CAD screening, CardioNets even surpassed the CMR-based model. In the MIMIC dataset, which included four conditions (CAD, heart failure, cardiomyopathy, and pulmonary arterial hypertension), CardioNets consistently exhibited strong performance. Except for heart failure, CardioNets outperformed the pretrained ECG model across all other diseases—for example, achieving a 2.5% improvement in pulmonary arterial hypertension screening. To further assess model generalizability, we applied the cardiomyopathy classification model trained on the MIMIC dataset directly to the FAHZU and SAHZU cohorts. CardioNets continued to outperform the pretrained ECG model in both external datasets, suggesting that the alignment between ECG and CMR enables the ECG encoder to effectively capture structural information inherent in CMR. This alignment enhances the ECG model’s performance across diverse datasets.

Label efficiency refers to the amount of training data and labels required to achieve a target performance level for a specific downstream task, highlighting the annotation workload for medical experts. CardioNets demonstrated remarkable label efficiency across various disease screening tasks in the MIMIC dataset (Fig. 3c). Notably, CardioNets achieved performance comparable to standalone scratch ECG models while using only 10% of the training data, underscoring the potential to address data scarcity. This capability is crucial for real-world applications, as it alleviates the annotation burden on clinical experts, making the model more applicable across diverse healthcare settings.

The CVD screening results reported in Fig. 3 were obtained by fine-tuning and evaluating models using all available positive samples and a randomly selected, approximately equal number of negative samples. While this facilitates controlled comparisons, it may not fully reflect real-world clinical settings. To better assess the performance of CardioNets under more realistic class imbalance conditions, we

evaluated the models using varying negative-to-positive sample ratios of 1:1, 2:1, 5:1, and 10:1 (Extended Fig. 1). Except for the scratch-trained ECG model, the AUC performance of CardioNets, the pretrained ECG model, and the CMR reference remained relatively stable across different imbalance ratios. Notably, CardioNets achieved performance comparable to the CMR reference and consistently outperformed the pretrained ECG model, highlighting its robustness and superior performance in imbalanced data scenarios.

In addition, we report the statistical comparisons of CardioNets against CMR reference, pretrained ECG, and scratch ECG models in terms of balanced accuracy (BA), mean average precision (mAP), and AUC (Extended Figs. 2–4). P-values between models were calculated using permutation tests, with $N = 10,000$ permutations conducted for each pairwise comparison. We also present the performance gain of CardioNets over each baseline method along with the corresponding sample size (n).

Comprehensive results, including sensitivity, specificity, accuracy, positive predictive value (PPV), negative predictive value (NPV), and F1-score, are provided in Supplementary Tables 1–6. All statistical significance analyses, including 95% confidence intervals and effect size metrics, are provided in the Supplementary Files.

Screening for subtypes of cardiomyopathy

We evaluated our model’s performance on the FAHZU dataset to assess its effectiveness in enhancing cardiomyopathy screening. The FAHZU dataset comprises 2,782 samples, including 1,705 cases of dilated cardiomyopathy (DCM), 915 cases of hypertrophic cardiomyopathy (HCM), and 162 cases of restrictive cardiomyopathy (RCM). Fig. 4 presents the results of five-fold cross-validation using CardioNets, pretrained ECG, and scratch ECG models, with classification performance shown using a one-vs-rest (OvR) approach. Compared to DCM and HCM, classification performance for RCM was notably lower when using the pretrained and scratch ECG models, likely due to the limited number of cases. However, CardioNets achieved the greatest improvement in RCM classification, reaching an AUC of 93.4%. Confusion matrix analysis further confirms that CardioNets offers superior discriminative ability for rare cardiomyopathy subtypes. These results underscore the strong generalization ability of CardioNets, particularly in accurately identifying rare cardiomyopathy subtypes with limited training samples.

In addition, statistical comparisons between CardioNets and baseline models (pretrained ECG, and scratch ECG) in terms of balanced accuracy, mean average precision (mAP), and AUC are reported in Extended Fig. 5. Comprehensive metrics—including sensitivity, specificity, accuracy, PPV, NPV, and F1-score—are available in Supplementary Tables 7, with all significance analyses detailed in the Supplementary Files.

Interpretation study and evaluation of CMR generation

To investigate the interpretability gained through ECG–CMR alignment, we employed the similarity matrix heatmap approach proposed in MMCL⁴¹ to compare CardioNets with the pretrained ECG and scratch ECG models (Fig. 5a). The results show that, after alignment with CMR, CardioNets exhibited higher cosine similarity between ECG signals and cardiac regions in the CMR images, while showing lower similarity with peripheral, less relevant areas. In contrast, the similarity matrices of the pretrained and scratch ECG models revealed more scattered attention patterns without clear focus.

This suggests that CardioNets learned to concentrate on cardiac-relevant regions and to disregard areas less meaningful for downstream tasks. These findings indicate that CardioNets effectively captures CMR-derived structural information to guide downstream predictions. Additional interpretability comparisons are provided in the Supplementary Files.

The CMR images generated by CardioNets preserve key physiological structures such as the myocardium and valves, as well as phenotype-related indicators commonly derived from CMR, including left ventricular myocardial mass (Fig. 5c). To evaluate the quality of the synthesized CMR images, we report both qualitative and quantitative results (Fig. 5b). A pretrained CMR encoder was used to extract features from both generated and real CMR images in the test set. These features were then visualized and compared using t-distributed stochastic neighbour embedding (t-SNE), a dimensionality reduction technique, to assess the similarity of their distributions in a lower-dimensional space. As shown in Fig. 5b, the t-SNE plots, histograms, and cumulative distribution function (CDF) plots reveal no substantial differences in feature distributions between generated and real CMR images. To further assess generation quality, we calculated structural similarity index (SSIM), peak signal-to-noise ratio (PSNR), mean absolute error (MAE), and root mean squared error (RMSE) between each synthesized CMR and its paired ground truth. We compared the performance of CardioNets against models based on cross-modal autoencoders²⁴ and diffusion-based²⁷ methods, and found that CardioNets consistently outperformed all baselines across these metrics. The structural and distributional consistency of the generated images lays a solid foundation for clinical interpretability and potential diagnostic support. Additional generation results are provided in the Supplementary Files.

Reader Study

To evaluate our AI model's performance in a real-world clinical setting, we conducted a reader study with an independent testing set of 111 subjects (77 cardiomyopathy patients and 34 controls) from The First Affiliated Hospital of Zhejiang University School of Medicine in 2024. The set was designed to be unselected, reflecting true clinical prevalence. The study had two stages. In the first, six physicians (two resident physicians, two attending physicians, and two associate chief physicians) assessed each patient for cardiomyopathy using only ECG signals. After a one-month washout, the second stage provided both real and AI-generated CMR images for re-evaluation.

As shown in Fig. 6a, most physicians exhibited limited screening performance when using ECG alone. The addition of AI-generated CMR notably improved diagnostic performance for resident and attending physicians. Across all participants, the combination of ECG and real CMR yielded the highest screening performance among human readers. However, it still fell short of CardioNets, which achieved the best performance with an AUC of 0.897. Fig. 6b presents the confusion matrices illustrating the ability of resident and attending physicians versus associate chief physicians to distinguish real from generated CMR images. The associate chief physicians more frequently misclassified real CMR images as AI-generated ones, likely due to their greater reliance on empirical experience and subjective interpretation - which, to some extent, demonstrates that the generated CMR images achieved such realistic quality that they could effectively confuse even expert judgment. In Fig. 6c, we compared the accuracy, sensitivity, specificity, and F1-score between all human physicians using ECG plus real CMR and CardioNets using ECG only. CardioNets demonstrated substantial improvements, achieving an accuracy 13.9% higher than the human average. Moreover, model inference is both faster and more cost-effective than physicians, offering a scalable and economical solution for large-scale population screening.

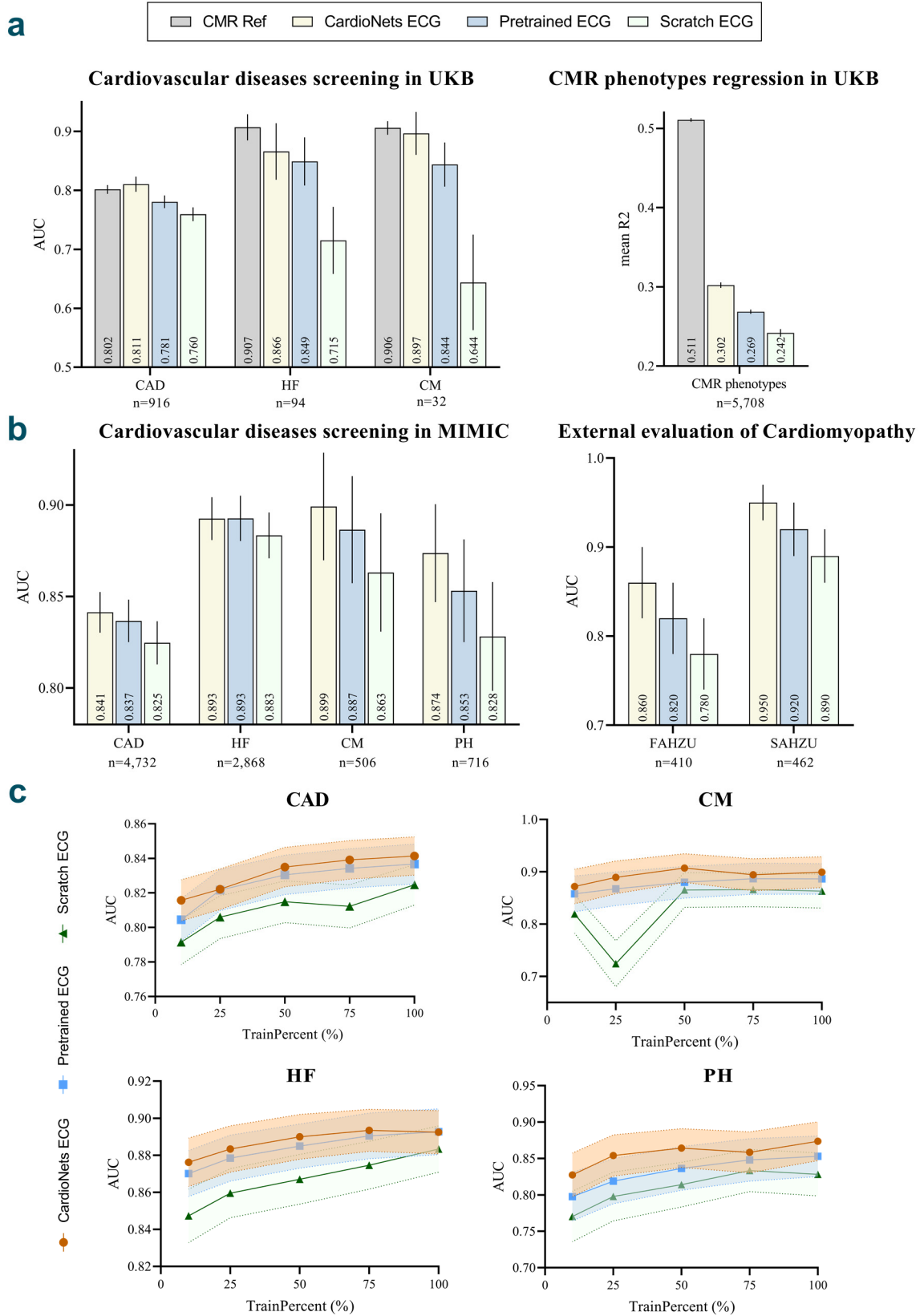


Fig. 3: Overall assessment of cardiovascular status and label utilization efficiency. a. The classification AUC metrics for coronary artery disease (CAD), cardiomyopathy (CM) and heart failure (HF), along with the average R2 values for cardiac structural phenotypes, were assessed in the UKB dataset. CardioNets was

evaluated against three types of models: ECG models trained from scratch, ECG models fine-tuned from pretrained encoders, and CMR-based models trained from SSL-pretrained encoders. **b.** Screening of CVDs, including CAD, CM, HF, and pulmonary hypertension (PH), in the MIMIC dataset, and external validation for cardiomyopathy screening. Due to the absence of corresponding CMR images in the MIMIC dataset, we compared CardioNets with ECG-based models. Both panel **a** and panel **b** report n as the number of samples in the test set. **c.** Label efficiency was analyzed by measuring the model’s performance with varying fractions of training data, providing insight into the amount of data required to achieve target performance levels.

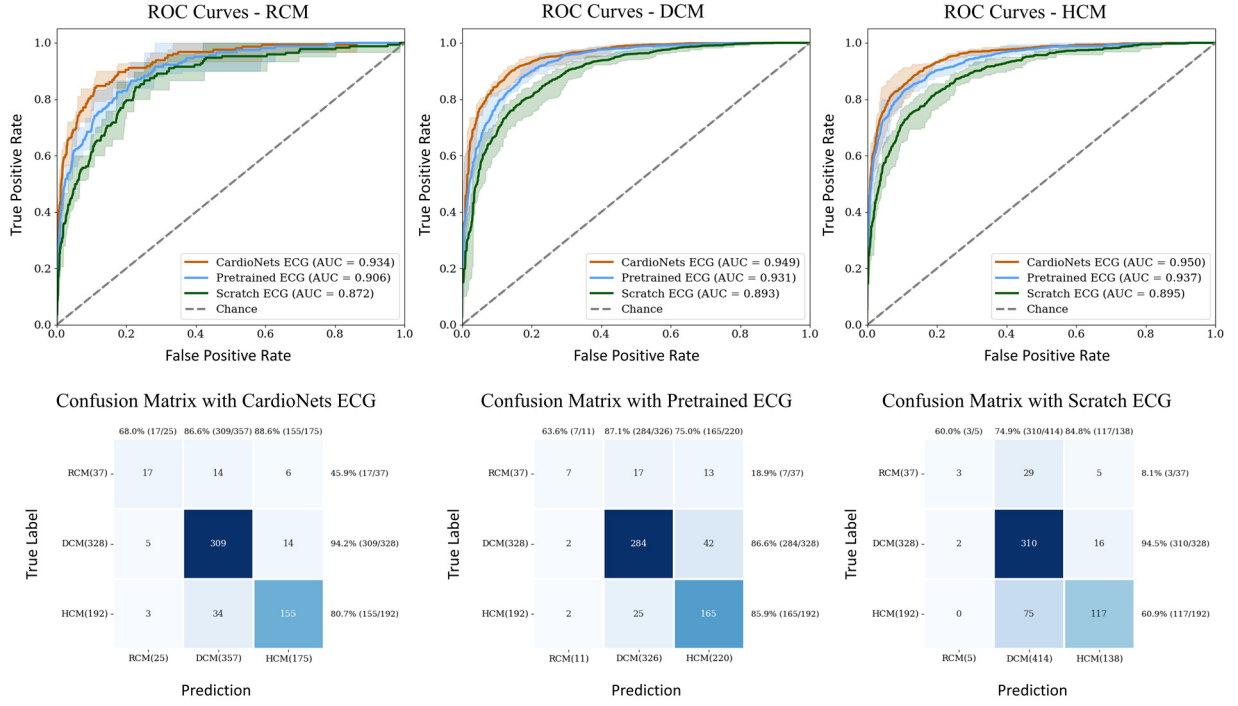


Fig. 4: Classification results of the three subtypes of cardiomyopathy in FAH2U.

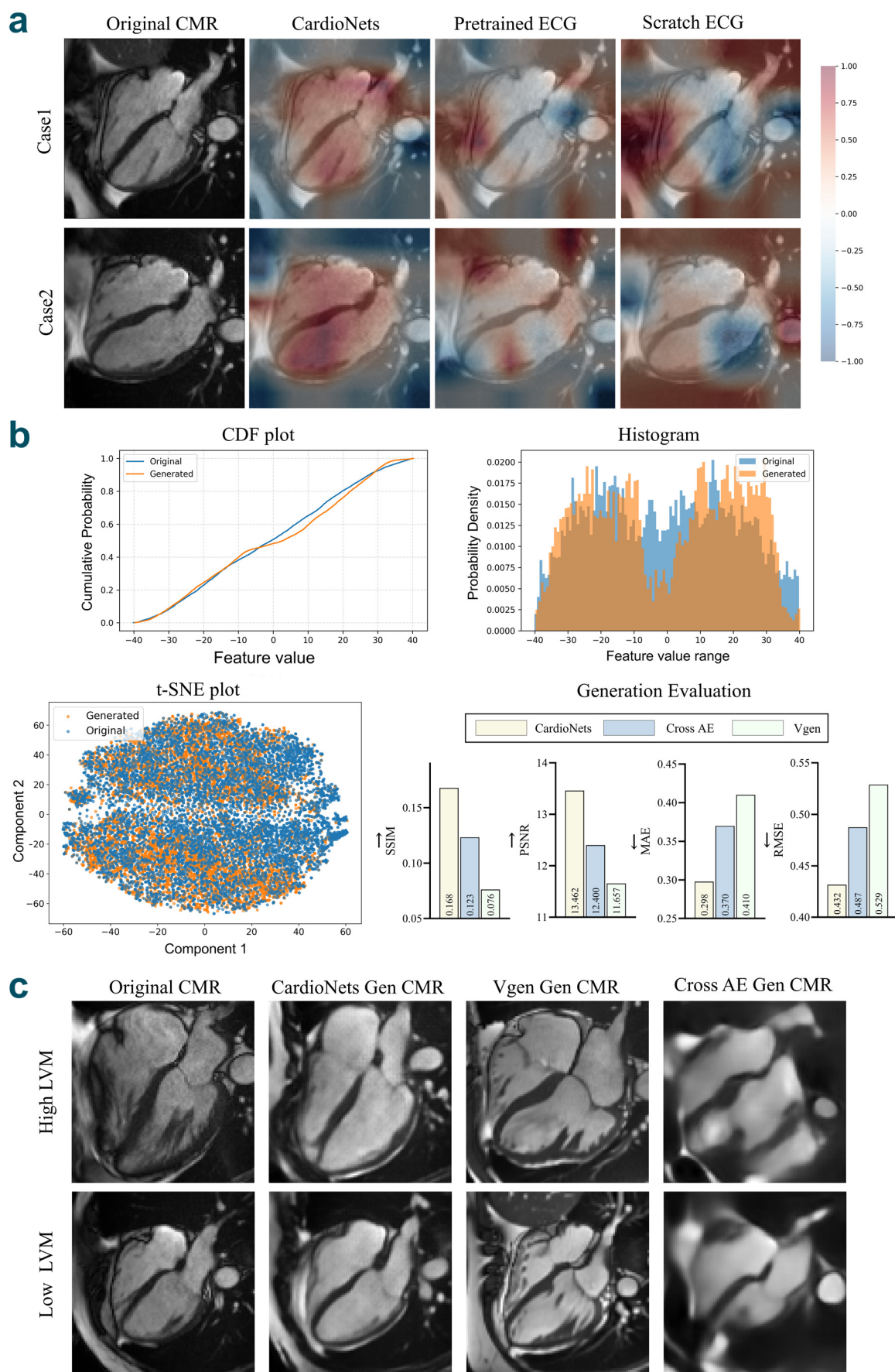


Fig. 5: Interpretability heatmap of CMR and quality assessment of generated CMR images. a. Cosine

similarity heatmaps of CardioNets, Pretrained ECG, and Scratch ECG, CardioNets shows a greater interest in CMR cardiac regions. **b.** Comparison of feature consistency and paired quantitative metrics (SSIM, PSNR, MAE, RMSE) between CardioNets-generated and real CMR images. **c.** Comparison of CMR images generated by CardioNets, Vgen, and Cross-AE for cases with high and low left ventricular myocardial mass.

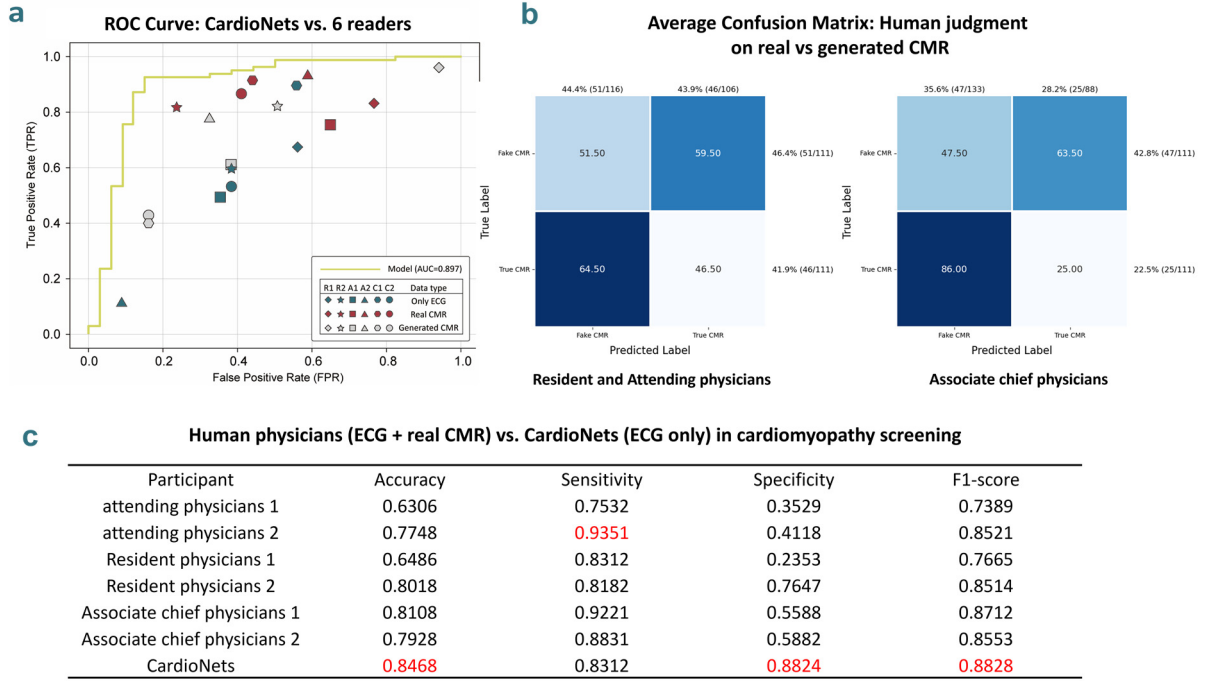


Fig. 6: Reader study. **a.** Performance of AI models and physicians in detecting cardiomyopathy across two stages: the first stage involved screening based solely on ECG interpretation, while the second stage provided physicians with either AI-generated or real CMR images. The reader study included two resident physicians (R1–R2), two attending physicians (A1–A2), and two associate chief physicians (C1–C2). **b.** Confusion matrix of physicians distinguishing generated from real CMR images. **c.** Comparison between human physicians using ECG and true CMR for cardiomyopathy screening and CardioNets using ECG alone.

Discussion

In this study, we propose CardioNets, a cross-modal pretraining model that employs a pretraining-finetuning paradigm to efficiently adapt to the screening of a broad spectrum of CVDs. Additionally, the visualizations generated by the model bolster the interpretability of the results. CardioNets demonstrates substantial potential for utilizing ECG in the screening of CVDs, particularly in economically underdeveloped regions where access to advanced diagnostic tools may be limited.

Building on our previous work²⁵, we acknowledge that while focusing on a specific task and obtaining CMR model weights through supervised learning can enhance the ECG model’s performance using contrastive loss training, this approach has a significant limitation: it does not leverage the inherent paired information between ECG and CMR. As a result, each time a new task arises, we must retrain both the CMR supervised model and the ECG alignment model specifically for that task. To address this limitation, we developed a model that introduces a critical shift from prior approaches: we utilize a self-supervised⁴² method to comprehensively learn the structural information of CMR. This encapsulates a

holistic representation of cardiac status that serves as a foundation for analyzing downstream tasks. In our self-supervised pretraining model, we freeze the parameters of the CMR model and update the ECG model by minimizing contrastive loss. This allows the ECG model to extract essential features that represent the overall cardiac state inherent to CMR, independent of specific tasks. These features exhibit strong discriminative capabilities across various downstream tasks. For CMR, we designed and developed a method called CPGG³², which generates large-scale synthetic CMR images for data augmentation by training a mask-based autoregressive generative model conditioned on cardiac phenotypes. These synthetic images are then used in a masked self-supervised learning framework³³ for pretraining, enabling the extraction of more robust CMR features that enhance downstream task performance. For ECG, which is inherently a periodic time-series signal, we employ a modified ViT⁴³ for encoding. This enables attention computation across independent blocks, allowing for a more comprehensive focus on information compared to traditional time-series models such as Recurrent Neural Networks (RNNs)⁴⁴.

The results of CardioNets on the UKB and MIMIC datasets demonstrate that the model significantly enhances the performance of ECG, particularly in smaller datasets, approaching the upper limits achieved through supervised learning with CMR. In contrast, this improvement is less pronounced in larger datasets, which is understandable: deep learning methods rely on large sample sizes to accurately approximate true distributions; therefore, the more data available, the better the model’s fitting capacity⁴⁵. However, even within the MIMIC dataset, where the number of samples for CAD and HF exceeds three to four thousand, models trained using ECG-CMR paired learning consistently outperform those based solely on supervised learning with ECG. This observation indicates that there is an upper limit to what can be achieved with ECG alone, primarily due to the lack of cross-modal structural information that CMR provides. This underscores the effectiveness of our cross-modal solution.

Interpretability is essential in clinical settings⁴⁶, and CardioNets introduces a masked autoregressive model conditioned on ECG to generate temporal CMR images. This approach allows for the creation of CMR images even in the absence of actual CMR data, serving as a valuable tool for both explainability and visualization. While existing video diffusion models, such as Sora⁴⁷, have made significant advances in areas like artistic creation, their use in medical imaging is still limited. This limitation arises from two main factors: first, the differing domain requirements: medicine prioritizes evidence-based practices⁴⁸ over creativity, which contrasts with the objectives of mainstream video diffusion models. Second, medical datasets often consist of only hundreds or thousands of samples⁴⁹, making it difficult to fully harness the potential of these models. Specifically, we leverage the generative model within CardioNets as an interpretable tool that provides physicians with enhanced explainability and visualization. By utilizing the aligned ECG encoder as a precise guide and training the generative model with a large-scale cross-modal dataset of approximately 40,000 samples, we achieve the generation of high-resolution, high-fidelity CMR images. Moreover, these images can effectively capture specific cardiac structural information (Fig. 5).

There is substantial evidence indicating that the most commonly used screening tests for cardiovascular disease—ECG and echocardiography—capture only a limited amount of the diagnostic information necessary for effective CVD anomaly detection^{50,51}. In contrast, CMR is regarded a common and effective diagnostic tool for CVDs⁵². However, CMR presents significant challenges in large-scale disease screening due to the complexities of cardiac motion, intricate operational procedures, and high

examination costs¹⁷. This naturally raises the question of whether ECG, which is simpler and more accessible, could be used as a substitute for CMR in CVD screening. The introduction of CardioNets demonstrates high performance across a range of downstream tasks, which shows that the model can extract and represent comprehensive cardiac information, including certain structural features, from CMR using only ECG data. It allows individuals to assess their cardiovascular health and disease risk through routine examinations in simplified community hospital settings, ultimately reducing the risks associated with delayed treatment.

Our study demonstrates that ECG can not only be used to screen for cardiomyopathy but also effectively identify its three subtypes. Cardiomyopathy is typically regarded as an irreversible heart disease⁵³, and distinct subtypes exhibit significant differences in cardiac structure and morphology⁵³. These differences necessitate distinct treatment and prognostic approaches tailored to each subtype⁵⁴. Therefore, early screening of cardiomyopathy subtypes is essential to support precision medicine and slow disease progression. In clinical diagnosis, precise identification of cardiomyopathy subtypes typically requires a comprehensive diagnostic workflow: the initial step usually involves CMR screening to categorize subtypes⁵⁵, followed by a second step involving myocardial biopsy or genetic test⁵⁶ for biomarker extraction to confirm the diagnosis. Given the complexity of cardiomyopathy, the diagnostic process for its subtypes resembles a branching structure rather than a linear pathway⁵⁷, making CMR-based screening indispensable as a first step. The proposed solution can provide early probabilistic classification of cardiomyopathy subtypes using ECG alone (Fig. 4). This finding highlights the potential for our model to replace CMR in subtype diagnosis, thereby streamlining the diagnostic process and conserving medical resources.

In the reader study, CardioNets, utilizing only ECG input, performed better to associate chief physicians evaluating both ECG and CMR, while significantly outperforming those who relied solely on ECG data. While our model achieves a favourable balance between specificity and sensitivity, as indicated by a high AUC, it is necessary to integrate the diagnostic logic of physicians into the model learning for enhancing human-machine interaction and fusion, potentially boosting the model's interpretability and clinical utility.

Several limitations must be considered. Firstly, while we validated the effectiveness of our solution using datasets from the UK, USA, and China, our pretrained model is based on approximately 40,000 ECG-CMR paired samples from the UK Biobank, which contains potential racial and socioeconomic biases⁵⁸. Therefore, it is essential to retrain or update our model using a more diverse population and to conduct a thorough analysis of how well the model generalizes to underrepresented cohorts before applying it in clinical settings. Additionally, while the current CardioNets demonstrates capability in the coarse classification of the three principal cardiomyopathy categories, it exhibits limited discriminative power for specific subtypes, including but not limited to cardiac amyloidosis, Fabry disease, and glycogen storage disease. This highlights the need for further model refinement to enhance its performance across a broader range of cardiomyopathy subtypes. Secondly, while our model generates high-fidelity CMR from ECG, further research is needed to understand how ECG influences the generative model to generate accurate CMR images. Finally, prospective validation in diverse cohorts is needed to assess generalizability, and integrating clinician diagnostic logic into model training could enhance human-machine collaboration. Future work will explore real-world deployment in community hospitals to evaluate scalability and equity gains.

In conclusion, CardioNets demonstrates the potential of cross-modal learning for cardiac assessment using only ECG, paving the way to enhance disease screening at the population level. The model's successful application in the ECG-CMR domain also highlights its potential for analysing other paired datasets with strong-weak modality relationships, opening new avenues for multimodal research across diverse medical contexts.

Competing Interests

The authors declare no competing interests.

Acknowledgements

The authors thank all study participants and staff for contributing to the UK Biobank Cohort under application number 89757.

Data availability

The data used in the study that supports cross-modal pre-training were obtained from the UK Biobank under application number 89757. Access to the UK Biobank data is available to all researchers with approval (<https://www.ukbiobank.ac.uk/enable-your-research/register>). The data used in the study that supports downstream tasks were obtained from the MIMIC-IV-ECG database, accessible via PhysioNet under credentialed access (<https://physionet.org/content/mimic-iv-ecg/1.0/>).

For the data from two private hospitals, the requirement for informed consent was waived by the respective ethics committees and institutions. The de-identified data can be shared only for non-commercial academic purposes and will require a formal material transfer agreement and a data use agreement. Requests should be submitted by emailing the corresponding authors (ZH, HZ, or TC) at zhengxinghuang@zju.edu.cn, doczhk@163.com, or ct010151452@zju.edu.cn. All requests will be evaluated based on institutional policies to determine whether the requested data are subject to intellectual property or patient privacy obligations. Generally, all such requests for access to data will be responded to within 1 month.

Code availability

The source codes about this study and data analysis in this manuscript are provided at <https://github.com/Yukui-1999/ECG-CMR>.

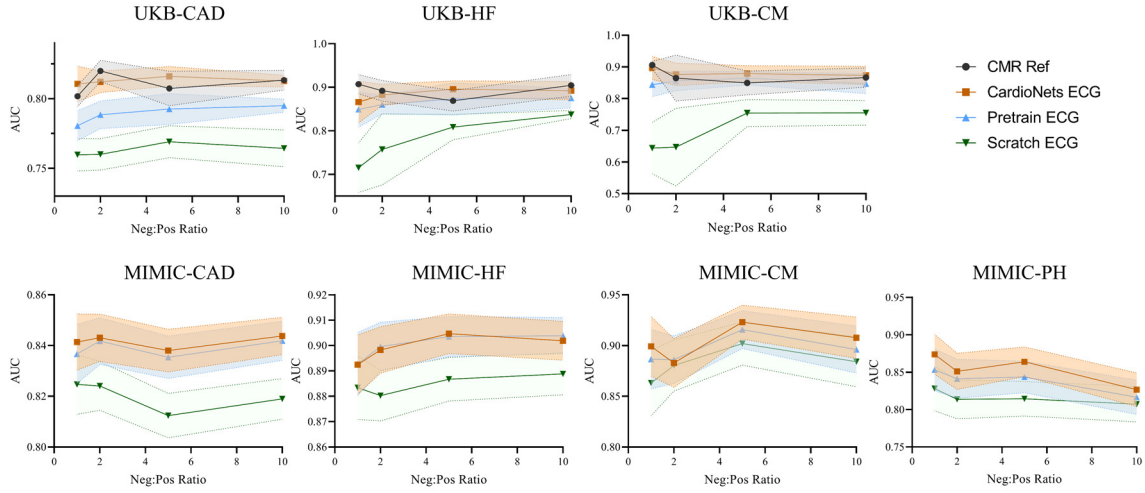
Funding

This work was supported by the Technical Innovation key project of Zhejiang Province (2024C03023), National Nature Science Foundation of China (Grant No. 82272129, 82470428).

Author contributions

ZH, HZ and FW jointly supervised research. ZH designed this study. ZD, ZY Li, and YH developed a deep learning model and performed the model interpretation. ZD, ZY Li, YM and HL performed data analysis. ZD, YH, ZK Li, WP, ZY Liu, XC, FW, TC, HZ and ZH interpreted the results. TC, QL, JW, YC, MC, LW, YX and CZ participated in the reader study. ZD, ZY Li, YH, TC and ZH prepared the first draft of the manuscript. All authors contributed and approved the final draft.

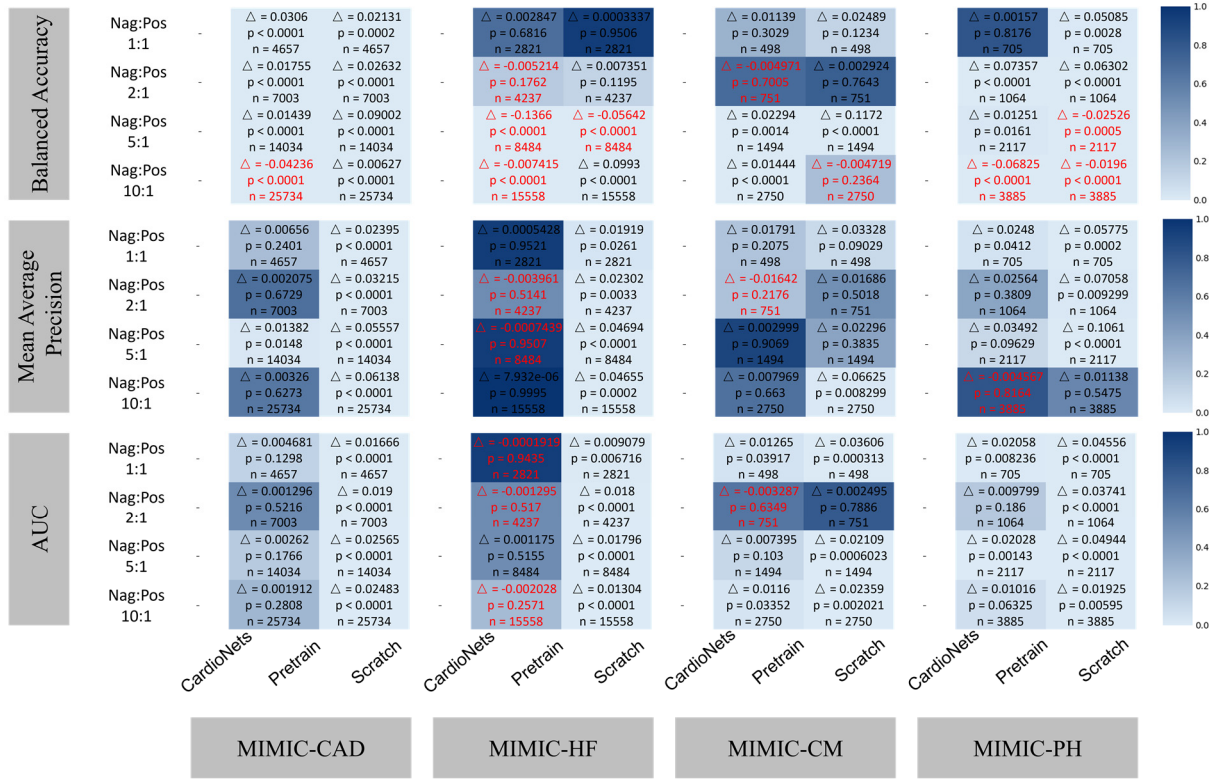
Extended Fig



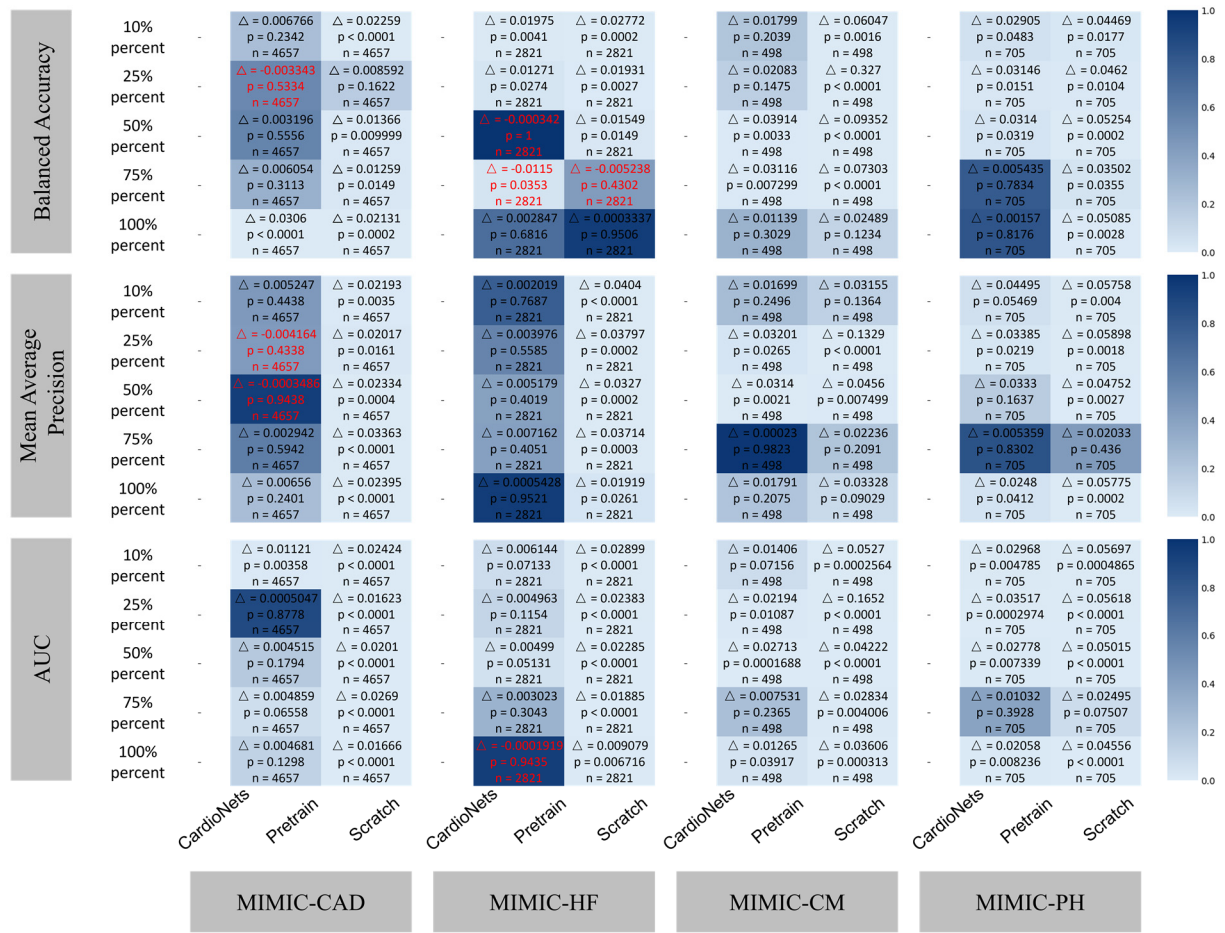
Extended Fig. 1: Comparison of AUCs for different cardiovascular diseases under varying negative/positive ratios in MIMIC and UKB datasets.

		UKB-CAD				UKB-HF				UKB-CM				
		CMR Ref	CardioNets	Pretrain	Scratch	CMR Ref	CardioNets	Pretrain	Scratch	CMR Ref	CardioNets	Pretrain	Scratch	
Balanced Accuracy	Nag:Pos 1:1	$\Delta = 0.008519$ $p = 0.2357$ $n = 4578$	$\Delta = 0.02621$ $p < 0.0001$ $n = 4578$	$\Delta = 0.04107$ $p < 0.0001$ $n = 4578$	$\Delta = -0.002137$ $p = 1$ $n = 468$	$\Delta = 0.03205$ $p = 0.06009$ $n = 468$	$\Delta = 0.1603$ $p < 0.0001$ $n = 468$	$\Delta = 0.04321$ $p = 0.3285$ $n = 162$	$\Delta = 0.02469$ $p = 0.6209$ $n = 162$	$\Delta = 0.3333$ $p < 0.0001$ $n = 162$				
	Nag:Pos 2:1	$\Delta = 0.009284$ $p = 0.1009$ $n = 6867$	$\Delta = 0.02119$ $p < 0.0001$ $n = 6867$	$\Delta = 0.07416$ $p < 0.0001$ $n = 6867$	$\Delta = 0.02991$ $p = 0.0262$ $n = 702$	$\Delta = 0.07372$ $p < 0.0001$ $n = 702$	$\Delta = 0.1186$ $p < 0.0001$ $n = 702$	$\Delta = 0.04321$ $p = 0.1554$ $n = 243$	$\Delta = 0.04012$ $p = 0.1531$ $n = 243$	$\Delta = 0.2963$ $p < 0.0001$ $n = 243$				
	Nag:Pos 5:1	$\Delta = -0.003801$ $p = 0.1414$ $n = 13734$	$\Delta = 0.03744$ $p < 0.0001$ $n = 13734$	$\Delta = 0.09594$ $p < 0.0001$ $n = 13734$	$\Delta = 0.04103$ $p < 0.0001$ $n = 1404$	$\Delta = 0.00034$ $p < 0.0001$ $n = 1404$	$\Delta = 0.2103$ $p < 0.0001$ $n = 1404$	$\Delta = 0.008642$ $p = 0.5151$ $n = 486$	$\Delta = -0.004938$ $p = 0.6165$ $n = 486$	$\Delta = 0.07778$ $p < 0.0001$ $n = 486$				
	Nag:Pos 10:1	$\Delta = -0.01114$ $p < 0.0001$ $n = 25179$	$\Delta = 0.02232$ $p < 0.0001$ $n = 25179$	$\Delta = 0.05242$ $p < 0.0001$ $n = 25179$	$\Delta = 0.0154$ $p = 0.0154$ $n = 2574$	$\Delta = 0.04509$ $p < 0.0001$ $n = 2574$	$\Delta = 0.1274$ $p < 0.0001$ $n = 2574$	$\Delta = 0.05247$ $p < 0.0001$ $n = 891$	$\Delta = 0.1525$ $p < 0.0001$ $n = 891$	$\Delta = 0.1772$ $p < 0.0001$ $n = 891$				
Mean Average Precision	Nag:Pos 1:1	$\Delta = -0.005457$ $p = 0.4346$ $n = 4578$	$\Delta = 0.0405$ $p < 0.0001$ $n = 4578$	$\Delta = 0.0621$ $p < 0.0001$ $n = 4578$	$\Delta = -0.03061$ $p = 0.1237$ $n = 468$	$\Delta = 0.0512$ $p = 0.05739$ $n = 468$	$\Delta = 0.168$ $p < 0.0001$ $n = 468$	$\Delta = 0.0007871$ $p = 0.9811$ $n = 162$	$\Delta = 0.1045$ $p = 0.0049$ $n = 162$	$\Delta = 0.321$ $p < 0.0001$ $n = 162$				
	Nag:Pos 2:1	$\Delta = -0.002354$ $p = 0.7843$ $n = 6867$	$\Delta = 0.03574$ $p < 0.0001$ $n = 6867$	$\Delta = 0.0872$ $p < 0.0001$ $n = 6867$	$\Delta = -0.03706$ $p = 0.1376$ $n = 702$	$\Delta = 0.03629$ $p = 0.227$ $n = 702$	$\Delta = 0.1275$ $p = 0.0002$ $n = 702$	$\Delta = -0.04635$ $p = 0.4085$ $n = 243$	$\Delta = -0.007118$ $p = 0.9151$ $n = 243$	$\Delta = 0.3607$ $p < 0.0001$ $n = 243$				
	Nag:Pos 5:1	$\Delta = -0.01355$ $p = 0.07949$ $n = 13734$	$\Delta = 0.07506$ $p < 0.0001$ $n = 13734$	$\Delta = 0.1123$ $p < 0.0001$ $n = 13734$	$\Delta = 0.003967$ $p = 0.9062$ $n = 1404$	$\Delta = 0.09797$ $p = 0.0005$ $n = 1404$	$\Delta = 0.2039$ $p < 0.0001$ $n = 1404$	$\Delta = -0.01453$ $p = 0.7561$ $n = 486$	$\Delta = -0.01129$ $p = 0.8885$ $n = 486$	$\Delta = 0.2396$ $p < 0.0001$ $n = 486$				
	Nag:Pos 10:1	$\Delta = -0.04437$ $p < 0.0001$ $n = 25179$	$\Delta = -0.007725$ $p = 0.304$ $n = 25179$	$\Delta = 0.07306$ $p < 0.0001$ $n = 25179$	$\Delta = 0.04671$ $p = 0.1681$ $n = 2574$	$\Delta = 0.08923$ $p = 0.0006999$ $n = 2574$	$\Delta = 0.2143$ $p < 0.0001$ $n = 2574$	$\Delta = 0.03922$ $p = 0.5151$ $n = 891$	$\Delta = 0.1369$ $p = 0.0259$ $n = 891$	$\Delta = 0.2689$ $p < 0.0001$ $n = 891$				
AUC	Nag:Pos 1:1	$\Delta = -0.001991$ $p = 0.7326$ $n = 4578$	$\Delta = 0.03413$ $p < 0.0001$ $n = 4578$	$\Delta = 0.04849$ $p < 0.0001$ $n = 4578$	$\Delta = -0.02245$ $p = 0.1396$ $n = 468$	$\Delta = 0.04119$ $p = 0.00878$ $n = 468$	$\Delta = 0.1517$ $p < 0.0001$ $n = 468$	$\Delta = 0.03833$ $p = 0.2589$ $n = 162$	$\Delta = 0.08307$ $p = 0.01378$ $n = 162$	$\Delta = 0.4012$ $p < 0.0001$ $n = 162$				
	Nag:Pos 2:1	$\Delta = 0.01159$ $p = 0.03951$ $n = 6867$	$\Delta = 0.03362$ $p < 0.0001$ $n = 6867$	$\Delta = 0.04768$ $p < 0.0001$ $n = 6867$	$\Delta = -0.01763$ $p = 0.3047$ $n = 702$	$\Delta = 0.03381$ $p = 0.0547$ $n = 702$	$\Delta = 0.1108$ $p < 0.0001$ $n = 702$	$\Delta = -0.01254$ $p = 0.7239$ $n = 243$	$\Delta = -0.01048$ $p = 0.7274$ $n = 243$	$\Delta = 0.2918$ $p < 0.0001$ $n = 243$				
	Nag:Pos 5:1	$\Delta = -9.537e-05$ $p = 0.9826$ $n = 13734$	$\Delta = 0.03113$ $p < 0.0001$ $n = 13734$	$\Delta = 0.04988$ $p < 0.0001$ $n = 13734$	$\Delta = 0.007006$ $p = 0.6541$ $n = 1404$	$\Delta = 0.03997$ $p = 0.001794$ $n = 1404$	$\Delta = 0.07118$ $p < 0.0001$ $n = 1404$	$\Delta = 0.01657$ $p = 0.5272$ $n = 486$	$\Delta = 0.01027$ $p = 0.5502$ $n = 486$	$\Delta = 0.1274$ $p < 0.0001$ $n = 486$				
	Nag:Pos 10:1	$\Delta = -0.001841$ $p = 0.7275$ $n = 25179$	$\Delta = 0.003521$ $p = 0.3356$ $n = 25179$	$\Delta = 0.03335$ $p < 0.0001$ $n = 25179$	$\Delta = 0.008221$ $p = 0.008221$ $n = 2574$	$\Delta = 0.0268$ $p = 0.02123$ $n = 2574$	$\Delta = 0.05287$ $p < 0.0001$ $n = 2574$	$\Delta = 0.06861$ $p = 0.0346$ $n = 891$	$\Delta = 0.05338$ $p = 0.05356$ $n = 891$	$\Delta = 0.1894$ $p < 0.0001$ $n = 891$				

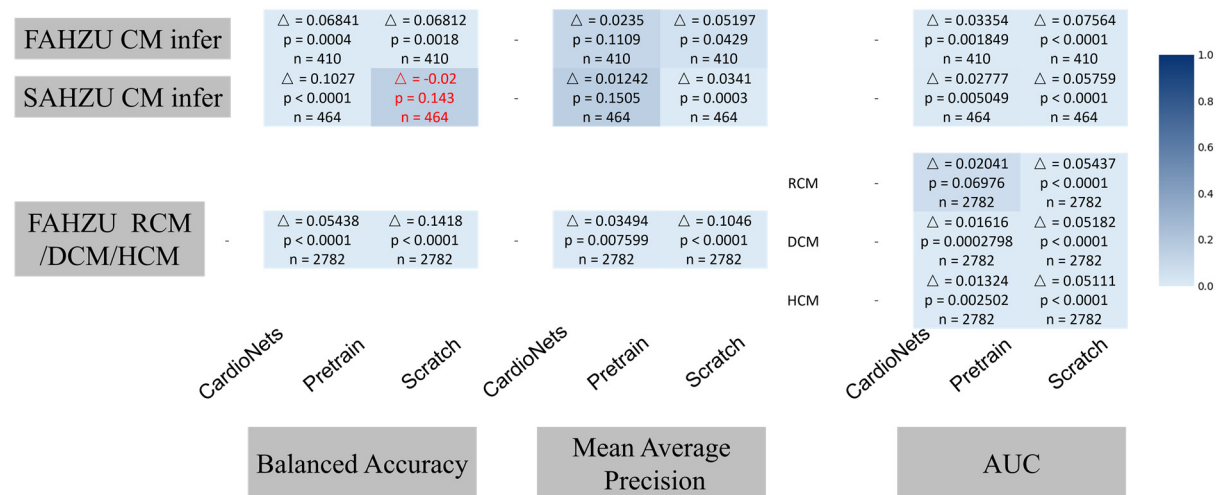
Extended Fig. 2: Detailed comparison of CardioNets against baseline methods—including CMR reference, pretrained ECG, and scratch ECG—for different cardiovascular diseases under varying negative-to-positive ratios in the UKB dataset. Each cell additionally reports the performance gain of CardioNets over the corresponding baseline (Δ), along with the sample size (n).



Extended Fig. 3: Detailed comparison of CardioNets against baseline methods—including pretrained ECG, and scratch ECG—for different cardiovascular diseases under varying negative-to-positive ratios in the MIMIC dataset. Each cell additionally reports the performance gain of CardioNets over the corresponding baseline (Δ), along with the sample size (n).



Extended Fig. 4: Detailed comparison of CardioNets against baseline methods—including pretrained ECG, and scratch ECG—for different cardiovascular diseases under different training set ratios in the MIMIC dataset. Each cell additionally reports the performance gain of CardioNets over the corresponding baseline (Δ), along with the sample size (n).



Extended Fig. 5: Performance comparison of CardioNets versus baseline methods—including pretrained ECG, and scratch ECG—for cardiomyopathy in FAUZH and SAHZU. Each cell additionally reports the performance gain of CardioNets over the corresponding baseline (Δ), along with the sample size (n).

References

1. Zhao, D. Epidemiological Features of Cardiovascular Disease in Asia. *JACC Asia* **1**, 1-13 (2021).
2. Timmis, A., *et al.* European Society of Cardiology: cardiovascular disease statistics 2021. *Eur Heart J* **43**, 716-799 (2022).
3. Tsao, C.W., *et al.* Heart Disease and Stroke Statistics-2023 Update: A Report From the American Heart Association. *Circulation* **147**, e93-e621 (2023).
4. Mortality, G.B.D. & Causes of Death, C. Global, regional, and national life expectancy, all-cause mortality, and cause-specific mortality for 249 causes of death, 1980-2015: a systematic analysis for the Global Burden of Disease Study 2015. *Lancet* **388**, 1459-1544 (2016).
5. Cheng, S., Han, Y., Jiang, L., Lan, Z. & Guo, J. National, regional, and global cardiomyopathy burden from 1990 to 2019. *Front Cardiovasc Med* **9**, 1042448 (2022).
6. Roth, G.A., *et al.* Global, Regional, and National Burden of Cardiovascular Diseases for 10 Causes, 1990 to 2015. *J Am Coll Cardiol* **70**, 1-25 (2017).
7. De Bacquer, D., De Backer, G., Kornitzer, M. & Blackburn, H. Prognostic value of ECG findings for total, cardiovascular disease, and coronary heart disease death in men and women. *Heart* **80**, 570-577 (1998).
8. Arnold, J.R. & McCann, G.P. Cardiovascular magnetic resonance: applications and practical considerations for the general cardiologist. *Heart* **106**, 174-181 (2020).
9. Rawi, A.A., Albashir, M.K. & Ahmed, A.M. Classification and detection of ECG arrhythmia and myocardial infarction using deep learning: a review. *Webology* **19**, 1151-1170 (2022).
10. Salerno, M. & Kramer, C.M. Advances in parametric mapping with CMR imaging. *JACC Cardiovasc Imaging* **6**, 806-822 (2013).
11. Jerosch-Herold, M. Quantification of myocardial perfusion by cardiovascular magnetic resonance. *J Cardiovasc Magn Reson* **12**, 57 (2010).
12. Friedrich, M.G. Tissue characterization of acute myocardial infarction and myocarditis by cardiac magnetic resonance. *JACC Cardiovasc Imaging* **1**, 652-662 (2008).
13. Rajiah, P.S., Francois, C.J. & Leiner, T. Cardiac MRI: State of the Art. *Radiology* **307**, e223008 (2023).
14. Ibrahim, E.H., *et al.* Value CMR: Towards a Comprehensive, Rapid, Cost-Effective Cardiovascular Magnetic Resonance Imaging. *Int J Biomed Imaging* **2021**, 8851958 (2021).
15. La Gerche, A., *et al.* Cardiac MRI: a new gold standard for ventricular volume quantification during high-intensity exercise. *Circ Cardiovasc Imaging* **6**, 329-338 (2013).
16. Salerno, M., *et al.* Recent Advances in Cardiovascular Magnetic Resonance: Techniques and Applications. *Circ Cardiovasc Imaging* **10**(2017).
17. Kim, R.J., *et al.* Guidelines for training in cardiovascular magnetic resonance (CMR). *J Cardiovasc Magn Reson* **20**, 57 (2018).
18. Sudlow, C., *et al.* UK biobank: an open access resource for identifying the causes of a wide range of complex diseases of middle and old age. *PLoS Med* **12**, e1001779 (2015).
19. Johnson, A.E.W., *et al.* MIMIC-IV, a freely accessible electronic health record dataset. *Sci Data* **10**, 1 (2023).
20. Radford, A., *et al.* Learning transferable visual models from natural language

- supervision. in *International conference on machine learning* 8748-8763 (PMLR, 2021).
21. Tian, K., Jiang, Y., Yuan, Z., Peng, B. & Wang, L. Visual autoregressive modeling: Scalable image generation via next-scale prediction. *Advances in neural information processing systems* **37**, 84839-84865 (2024).
 22. Li, T., Tian, Y., Li, H., Deng, M. & He, K. Autoregressive image generation without vector quantization. *Advances in Neural Information Processing Systems* **37**, 56424-56445 (2024).
 23. Rombach, R., Blattmann, A., Lorenz, D., Esser, P. & Ommer, B. High-resolution image synthesis with latent diffusion models. in *Proceedings of the IEEE/CVF conference on computer vision and pattern recognition* 10684-10695 (2022).
 24. Radhakrishnan, A., *et al.* Cross-modal autoencoder framework learns holistic representations of cardiovascular state. *Nat Commun* **14**, 2436 (2023).
 25. Ding, Z., *et al.* Cross-Modality Cardiac Insight Transfer: A Contrastive Learning Approach to Enrich ECG with CMR Features. in *International Conference on Medical Image Computing and Computer-Assisted Intervention* 109-119 (Springer, 2024).
 26. Turgut, Ö., *et al.* Unlocking the diagnostic potential of ecg through knowledge transfer from cardiac mri. *arXiv preprint arXiv:2308.05764* (2023).
 27. Wang, J., *et al.* Modelscope text-to-video technical report. *arXiv preprint arXiv:2308.06571* (2023).
 28. Gow, B., *et al.* Mimic-iv-ecg-diagnostic electrocardiogram matched subset. *Type: dataset* (2023).
 29. Zhou, Y., *et al.* A foundation model for generalizable disease detection from retinal images. *Nature* **622**, 156-163 (2023).
 30. Schafer, R.W. What is a savitzky-golay filter?[lecture notes]. *IEEE Signal processing magazine* **28**, 111-117 (2011).
 31. Bai, W., *et al.* A population-based phenome-wide association study of cardiac and aortic structure and function. *Nature medicine* **26**, 1654-1662 (2020).
 32. Li, Z., *et al.* Phenotype-Guided Generative Model for High-Fidelity Cardiac MRI Synthesis: Advancing Pretraining and Clinical Applications. *arXiv preprint arXiv:2505.03426* (2025).
 33. He, K., *et al.* Masked autoencoders are scalable vision learners. in *Proceedings of the IEEE/CVF conference on computer vision and pattern recognition* 16000-16009 (2022).
 34. Na, Y., Park, M., Tae, Y. & Joo, S. Guiding masked representation learning to capture spatio-temporal relationship of electrocardiogram. *arXiv preprint arXiv:2402.09450* (2024).
 35. Li, T., *et al.* Mage: Masked generative encoder to unify representation learning and image synthesis. in *Proceedings of the IEEE/CVF Conference on Computer Vision and Pattern Recognition* 2142-2152 (2023).
 36. Wilson, E.B. Probable inference, the law of succession, and statistical inference. *Journal of the American Statistical Association* **22**, 209-212 (1927).
 37. Van Der Walt, S., Colbert, S.C. & Varoquaux, G. The NumPy array: a structure for efficient numerical computation. *Computing in science & engineering* **13**, 22-30 (2011).
 38. Pedregosa, F., *et al.* Scikit-learn: Machine learning in Python. *the Journal of machine Learning research* **12**, 2825-2830 (2011).
 39. Virtanen, P., *et al.* SciPy 1.0: fundamental algorithms for scientific computing in Python. *Nature methods* **17**, 261-272 (2020).

40. Lowekamp, B.C., Chen, D.T., Ibáñez, L. & Blezek, D. The design of SimpleITK. *Frontiers in neuroinformatics* **7**, 45 (2013).
41. Turgut, Ö., *et al.* Unlocking the diagnostic potential of electrocardiograms through information transfer from cardiac magnetic resonance imaging. *Medical Image Analysis* **101**, 103451 (2025).
42. Krishnan, R., Rajpurkar, P. & Topol, E.J. Self-supervised learning in medicine and healthcare. *Nature Biomedical Engineering* **6**, 1346-1352 (2022).
43. Dosovitskiy, A. An image is worth 16x16 words: Transformers for image recognition at scale. *arXiv preprint arXiv:2010.11929* (2020).
44. Medsker, L.R. & Jain, L. Recurrent neural networks. *Design and Applications* **5**, 2 (2001).
45. Hestness, J., *et al.* Deep learning scaling is predictable, empirically. *arXiv preprint arXiv:1712.00409* (2017).
46. Tonekaboni, S., Joshi, S., McCradden, M.D. & Goldenberg, A. What clinicians want: contextualizing explainable machine learning for clinical end use. in *Machine learning for healthcare conference* 359-380 (PMLR, 2019).
47. Liu, Y., *et al.* Sora: A review on background, technology, limitations, and opportunities of large vision models. *arXiv preprint arXiv:2402.17177* (2024).
48. Sackett, D.L. & Rosenberg, W.M.C. On the need for evidence-based medicine. *Journal of Public Health* **17**, 330-334 (1995).
49. Schäfer, R., *et al.* Overcoming data scarcity in biomedical imaging with a foundational multi-task model. *Nature Computational Science* **4**, 495-509 (2024).
50. Valente, A.M., *et al.* Comparison of echocardiographic and cardiac magnetic resonance imaging in hypertrophic cardiomyopathy sarcomere mutation carriers without left ventricular hypertrophy. *Circulation: Cardiovascular Genetics* **6**, 230-237 (2013).
51. Capron, T., *et al.* Cardiac magnetic resonance assessment of left ventricular dilatation in chronic severe left-sided regurgitations: comparison with standard echocardiography. *Diagnostic and interventional imaging* **101**, 657-665 (2020).
52. Hundley, W.G., *et al.* ACCF/ACR/AHA/NASCI/SCMR 2010 expert consensus document on cardiovascular magnetic resonance: a report of the American College of Cardiology Foundation Task Force on Expert Consensus Documents. *Journal of the American College of Cardiology* **55**, 2614-2662 (2010).
53. Brieler, J., Breeden, M.A. & Tucker, J. Cardiomyopathy: an overview. *American family physician* **96**, 640-646 (2017).
54. Gimeno, J.R., *et al.* Prospective follow-up in various subtypes of cardiomyopathies: insights from the ESC EORP Cardiomyopathy Registry. *European Heart Journal-Quality of Care and Clinical Outcomes* **7**, 134-142 (2021).
55. Jan, M.F. & Tajik, A.J. Modern imaging techniques in cardiomyopathies. *Circulation research* **121**, 874-891 (2017).
56. McKenna, W.J., Maron, B.J. & Thiene, G. Classification, epidemiology, and global burden of cardiomyopathies. *Circulation research* **121**, 722-730 (2017).
57. Arbustini, E., *et al.* The MOGE (S) classification of cardiomyopathy for clinicians. *Journal of the American College of Cardiology* **64**, 304-318 (2014).
58. Obermeyer, Z., Powers, B., Vogeli, C. & Mullainathan, S. Dissecting racial bias in an algorithm used to manage the health of populations. *Science* **366**, 447-453 (2019).